PHYSICAL REVIEW B VOLUME 51, NUMBER 13 1 APRIL 1995-I

Secondary-ion-mass-spectroscopy study of oxygen tracer diffusion in a *c*-axis-oriented $YBa_2Cu_3O_{7-\delta}$ film

Yupu Li and J. A. Kilner
Department of Materials, Imperial College of Science Technology and Medicine, London SW7 2BP, United Kingdom

T. J. Tate and M. J. Lee
Department of Electronic and Electrical Engineering and Center for High Temperature Superconductivity, Imperial College of Science Technology and Medicine, London SW7 2BT, United Kingdom

R. J. Chater, H. Fox, and R. A. De Souza
Department of Materials, Imperial College of Science Technology and Medicine, London SW7 2BP, United Kingdom

P. G. Quincey
National Physical Laboratory, Teddington, Middlesex, TW11 0LW, United Kingdom
(Received 18 October 1994)

The atomic motion of oxygen in a *c*-axis-oriented $YBa_2Cu_3O_{7-\delta}$ film was studied with implanted ^{18}O as a tracer. Conventional annealing in an oxygen flowing ambient was performed for 1 hour at various temperatures between 175 and 550 °C. Analysis by secondary-ion mass spectroscopy shows that the implanted ^{18}O starts to migrate within the $YBa_2Cu_3O_{7-\delta}$ film at a low temperature, between 250 and 300 °C. Results from gas/solid oxygen isotopic exchange shows that at 315 °C oxygen can enter the $YBa_2Cu_3O_{7-\delta}$ film and confirms the high mobility of oxygen within the film even at this low temperature. The apparent volume diffusivity of the oxygen at 315 °C is found to be $\sim 1.5\times 10^{-13}$ cm^2/s. Short-circuit diffusion is thought to play an important role in determining the high mobility of oxygen in the *c*-axis-oriented $YBa_2Cu_3O_{7-\delta}$ film.

I. INTRODUCTION

Mass transport by diffusion is an important phenomenon in high-temperature superconductors (HTSC) since it controls such behavior as sintering, chemical reactivity, stoichiometry, transport properties, and damage by irradiation. It has been found that oxygen ordering in $YBa_2Cu_3O_{7-\delta}$ (YBCO) plays a very important role in superconductivity. The motion of oxygen has been a major focus in the literature. An activation energy of 1.2±0.2 eV for oxygen self-diffusion in the *a-b* plane and 1.6±0.3 eV for oxygen self-diffusion in the *c* direction, can be generally summarized from the published results,[1–6] together with an anisotropic factor $D_{a-b}/D_c \sim 10^4-10^6$. It should be noted that the above results were derived mainly from bulk single-crystal or polycrystalline YBCO samples (referred to as diffusion in the *a-b* plane).

Epitaxial YBCO films hold great promise for practical applications, but there are few data about diffusivity of oxygen in epitaxial YBCO films.[7–9] Assuming that the resistance change of the film is a consequence of oxygen diffusion, an activation energy of 0.33 eV has been reported, for the temperature range between 450 and 550 °C, for oxygen diffusion in a *c*-axis-oriented YBCO film produced by laser ablation.[8] Whereas by annealing of deoxygenated $YBa_2Cu_3O_x$ ($x=6.1-6.2$) in an oxygen atmosphere and following the change of oxygen content by x-ray measurement, Chen *et al.*[7] reported an activation energy of 1.23 eV for oxygen diffusion in *c*-axis-oriented $YBa_2Cu_3O_x$ films produced by electron beam and thermal evaporation. In addition, it has been reported that during the production of *c*-axis-oriented YBCO films by sputtering, a subsequent heat treatment in pure oxygen at about 430 °C for about 20 min can decrease the deficiency of oxygen.[10] This implies that the oxygen is highly mobile at such temperatures. However, at 430 °C over 20 min, the characteristic diffusion length $2\sqrt{Dt}$, for the *c* direction and the *a-b* plane yield 10 nm and 5.8 μm, respectively. Increasing the time from 20 min to 2 h does not significantly increase this "diffusion length." Thus the question arises, for *c*-axis-oriented YBCO films how can the oxygen ordering and/or enrichment be achieved at such low temperatures.

This work reports direct measurements of oxygen self-diffusion in the *c* direction of a sputtered *c*-axis-oriented YBCO film. Diffusion samples were formed by ion implantation of ^{18}O into the *c*-axis-oriented YBCO film with a thickness of ~ 830 nm. Isotopic gas-solid exchange has also been used for comparison.

SIMS analysis of such samples shows that oxygen is highly mobile in such *c*-axis-oriented YBCO films. The aim of this study is not only to gain an understanding of the fundamental aspects of oxygen migration in YBCO

0163-1829/95/51(13)/8498(5)/$06.00 51 ©1995 The American Physical Society

films, but also to find out practical annealing conditions for oxygen reordering in irradiated and treated YBCO films. We will report on the effects of conventional annealing and rapid thermal annealing on as-received and irradiated YBCO films in a separate paper.

II. EXPERIMENTAL

A YBCO film was deposited on a (100) $LaAlO_3$ single crystal *in situ* by dc sputtering from a stoichiometric target, using the inverted cylindrical magnetron method.[10] The sputtering gas pressure was 870×10^{-3} mbar, with a mixture of 2/3 argon and 1/3 oxygen. The substrate was clamped to a resistive heater, with a copper shim to improve thermal contact. During deposition of the film, the temperature of the heater block was 840 °C. After deposition the chamber was backfilled to 250 mbar of oxygen, and the sample allowed to cool to about 450 °C for 15 min before the heater was switched off. The film was ~830 nm thick, with a superconducting transition temperature of 90.5 K ($R=0$), as determined by both a dc resistance measurement and an inductive method.[11] X-ray diffraction (XRD) showed that the YBCO film was grown primarily with the c axis perpendicular to the substrate surface. The c-axis lattice parameter and inferred oxygen content $(7-\delta)$ were equal to 11.67 and 6.95 Å respectively. No a-axis-oriented grains could be found within the well-connected c-axis-oriented film, either by XRD or scanning electron microscopy (SEM) studies. The film was determined to be quite uniform, but usually such epitaxial YBCO films contain some second-phase precipitates and twin boundaries.

Irradiation was performed with 200 keV ^{18}O to a dose of $5\times10^{16}/cm^2$ at room temperature (RT), at 7° to the surface normal to minimize channeling effects. After implantation the sample was subdivided into pieces of size $\sim2\times3$ mm^2 and annealed for 1 h in a tube furnace in an oxygen flowing ambient, at various temperatures between 175 and 550 °C. For one of the pieces, sequential isochronal annealing was also performed. A further piece of the as-received film was used for isotopic gas-solid exchange. The sample was annealed at 315 °C for 1 h in a quartz tube containing ^{18}O at a pressure of 990 mbar. Details of the annealing schedules of samples referred to in this paper are listed in Table I.

Oxygen depth profiles after implantation and after each of the post-irradiation annealing steps were obtained on an Atomika 6500 SIMS instrument by using a 10 keV Cs^+ primary beam at normal incidence and analyzing the negative secondary ions. Details of the analysis of YBCO films using SIMS can be found in our previous publications.[12,13] The position of the interface between the YBCO film and the substrate can be easily inferred from the steps of $^{16}O^-$ and $^{63}Cu^-$ signals.[12] Oxygen isotopic fraction profiles were obtained from the intensity ratio $^{18}O^-/(^{18}O^-+^{16}O^-)$, these intensity ratios are used for comparisons between samples of different annealing condition and for estimation of the retained dose of ^{18}O in the film. It should be noted that the isotopic "background" of ^{18}O, obtained by taking the intensity ratio of $^{18}O^-/(^{18}O^-+^{16}O^-)$ at the end of the depth profiles, is equal to ~0.002, which corresponds well to the natural isotopic abundance. Because the original oxide contains ^{18}O at the natural abundance level of 0.002 prior to implantation, calculations of the retained dose using the area under the isotope ratio profile plots have this natural abundance level subtracted. Only changes larger than ±5% of the area under the isotopic ratio profile are detectable using this method, because the absolute quantification of the area is dependent on the measured depth which includes this level of error.

III. RESULTS AND DISCUSSIONS

As-implanted ^{18}O depth profile. Line 1 in Fig. 1 shows the as-implanted ^{18}O isotopic ratio profile for sample no. 2. The YBCO film, with a density of 6.54 g/cm^3, contains 4.1×10^{22} oxygen atom/cm^3. The natural abundance of the two most abundant oxygen isotopes is 99.8% ^{16}O and 0.2% ^{18}O. This means that 24.15 nm of $YBa_2Cu_3O_7$ film will thus correspond to 1×10^{17} O atom/cm^2. On average, the implanted ^{18}O corresponds to about 1.45% of oxygen already present in the oxygen sublattice of the 123 phase. Under the assumption that the density of the film is unchanged during implantation, the area (called Q_0 below) under the ^{18}O isotopic ratio

TABLE I. Details of the annealing schedule of the samples referred to in the text.

Sample no.	$^{18}O^+$ implant (200 keV, $5\times10^{16}/cm^2$)	Annealing condition
1	No	As received
2[a]	Yes	
3[a]	Yes	175 °C for 1 h, in flowing ^{16}O (1 bar)
4[a]	Yes	As 3+250 °C for 1 h, in flowing ^{16}O (1 bar)
5[a]	Yes	As 4+ 350 °C for 1 h, in flowing ^{16}O (1 bar)
6[a]	Yes	As 5+450 °C for 1 h, in flowing ^{16}O (1 bar)
7[a]	Yes	As 6+550 °C for 1 h, in flowing ^{16}O (1 bar)
8[a]	Yes	300 °C for 1 h, in flowing ^{16}O (1 bar)
9	Yes	315 °C for 1 h, in flowing ^{16}O (1 bar)
10	No	315 °C for 1 h, in ^{18}O (990 mbar)

[a]Samples were used for sequential isochronal annealing. For such samples, after each of the anneal steps the sample was cooled to room temperature for analysis, and then annealed again.

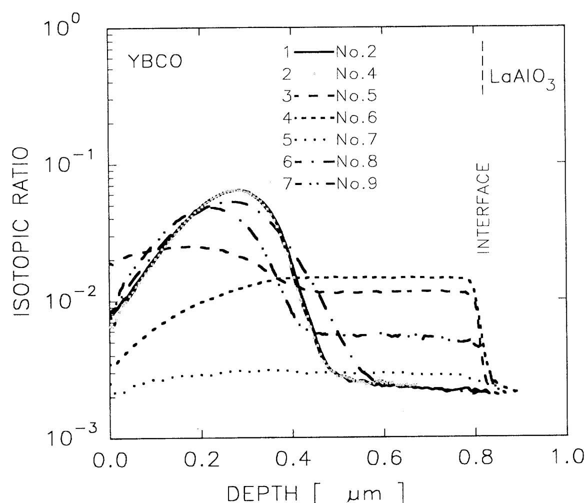

FIG. 1. Lines 1–7, ^{18}O isotopic ratio profiles for samples no. 2 and 4–9 listed in Table I.

curve, corrected for the natural abundance, represents the implanted ^{18}O and corresponds to a dose of $(5.6\pm0.3)\times10^{16}$ ^{18}O/cm^2, which is in good agreement with the nominal dose of 5×10^{16} ^{18}O/cm^2. Therefore, the concentration calibration of the as-implanted ^{18}O distribution shown by line 1 in Fig. 2 was achieved by assuming all the (nominal) implanted ^{18}O has been trapped in the sample. Lines 2 and 3 in Fig. 2 show the simulated ^{18}O and dpa (displacements per atom) depth profiles obtained by the PC-based code TRIM-92 (Ref. 14) which assumes a random target medium. For simulating these distributions a threshold displacement energy E_d of 20 eV for all elements is assumed. It can be seen that the agreement between the measured depth profile and simulated depth profile is good, although the range data (such as the mean projected range) for the measured depth profile are about 10% larger than those for the simulated

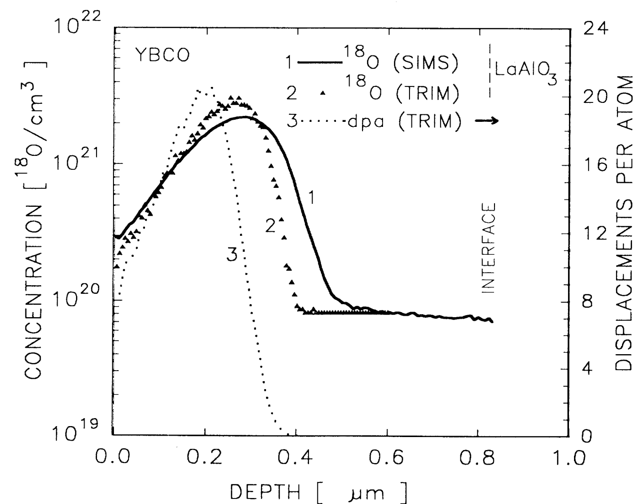

FIG. 2. Line 1, the as-implanted ^{18}O concentration distribution; lines 2 and 3, the simulated ^{18}O concentration and damage distributions for the YBCO film obtained by TRIM-92.

profile. Figure 2 shows that most of the displacement damage remains within the ~440 nm top layer of the film. Therefore, it can be expected that this irradiation will result in a surface amorphous layer (to a depth of ~420 nm). This corresponds to a dpa level of 0.2 for amorphizing the YBCO films by irradiation.[15–17] Here, we have considered that the actual damage distribution may be 10% deeper than that simulated, due to the measured range being 10% deeper. In addition, the deeper part of the film, at least 200 nm of the film adjacent to the interface contains less of both radiation damage and implanted ^{18}O.

^{18}O diffusion in the film during annealing. Lines 2–7 in Fig. 1 show the ^{18}O isotopic ratio profiles for samples nos. 4–9. The area (under the ^{18}O isotopic ratio curve *with* natural ^{18}O isotopic abundance subtracted) which corresponds to the retained dose of ^{18}O for each sample can be estimated to be $(98.1\pm5.0)\%$ Q_0, $(78.6\pm4.0)\%$ Q_0, $(51.6\pm2.6)\%$ Q_0, $(4.6\pm0.3)\%$ Q_0, $(95.5\pm4.8)\%$ Q_0, and $(84.8\pm4.3)\%$ Q_0, respectively. The area ratios of the ^{18}O isotopic ratio curve for each sample to the as-implanted ^{18}O isotopic ratio curve, *without* the natural ^{18}O isotopic abundance subtracted, are found to be ~98%, ~81%, ~57%, ~15%, ~96%, and ~87%, respectively. It is clear that the implanted ^{18}O plays a role in *monitoring* the oxygen migration within the film. However, it should be mentioned here that the change of the area under ^{18}O isotopic ratio curve during annealing is mainly due to the effect that ^{16}O in the gas ambient exchanges with ^{18}O within the film. Additionally, we must consider that the total oxygen content of the film may change during the annealing process, i.e., that some oxygen enrichment and/or indiffusion by oxidation or oxygen loss and/or outdiffusion by reduction may also induce a change of the area under the ^{18}O isotopic ratio curve. Calculations show that a 10% oxygen enrichment (or loss) of the film by the natural oxygen gas (99.8% ^{16}O) ambient will only induce 10% decrement (or increment) of the area and thus can only play a minor role in the change of the area under ^{18}O isotopic ratio curve. In fact, we do not think that such oxygen loss or enrichment as large as 10% takes place, for the following reason: (i) the as-received film is near fully oxidized; (ii) the implanted ^{18}O only corresponds to about 1.45% of oxygen already in the film; (iii) it is reasonable to assume that target atoms (such as oxygen) may be displaced rather than the oxygen being lost from the film[17,18] because within the irradiated film there are enough sinks for the displaced oxygen. This could induce locally disordered regions and hence locally induce a large change in the oxygen sublattice, such as from the superconducting $O_{6.95}$ to nonsuperconducting $O_{6.25}$ (and further to an amorphous film); (iv) the displaced oxygen can partly reorder accompanying the regrowth of the top amorphous YBCO layer or join the oxygen exchange during the anneals; (v) within this annealing temperature-oxygen pressure range the orthorhombic 123 phase should be stable.[19]

It is clear that up to 250 °C (see, for example, line 2 in Fig. 1) the implanted ^{18}O is immobile and no detectable oxygen has moved into, or out of, the film. In such a case, the possibility of oxygen entering the film and

remaining as atomic oxygen has also been ruled out, as the change of the total oxygen concentration will induce the change of the area and ^{18}O isotopic ratio profile. However, we cannot rule out the possibility of some O_2 moving into the film and remaining as O_2. At 300 °C the implanted ^{18}O is clearly mobile (see line 6 in Fig. 1). The profile becomes broader and some of the implanted ^{18}O migrates into the deeper layer of the film where the irradiation damaged is less. Using $\Delta X^2=2D_A t$ (i.e., via Brownian movement[20]), the apparent diffusion coefficient in the irradiated film, D_A, is $\sim 1.4\times 10^{-14}$ cm^2/s at 300 °C. Here, we have defined the mean-square displacement of the diffusing ^{18}O, ΔX^2, as equal to the difference between the square of the right half-height widths for line 6 and line 1 in Fig. 1.

For the higher temperatures (i.e., $T \geq 350$ °C), the final ^{18}O isotopic ratio profiles (see lines 3–5) are controlled by both effects of (i) the gas ^{16}O/solid ^{18}O exchange and diffusion in the surface layer accompanying the regrowth of the implanted layer and (ii) ^{18}O self-diffusion within the film. Clearly oxygen is highly mobile within the YBCO film at such high temperatures. ^{18}O self-diffusion within the film tends to make the ^{18}O distribute uniformly throughout the film, whereas gas ^{16}O-solid ^{18}O exchange and diffusion in the surface induces a dip in the ^{18}O isotopic ratio profile in the surface region, as shown, and a reduction in the total ^{18}O content of the film as defined by the area under the isotopic ratio curve.

In addition, no obvious evidence shows that ^{18}O is mobile across the interface between the film and the substrate at these temperatures. The diffusion coefficient of the oxygen in single-crystal $LaAlO_3$ is clearly much lower than that in the YBCO film (see, for example, the tails of lines 4–7).

^{18}O gas/^{16}O solid exchange. Line 1 in Fig. 3 shows the exchange and diffusion profile of ^{18}O for sample no. 10. Line 1 in the inset of Fig. 3 shows the same profile but the scale type of vertical axis is in common logarithm. Line 2 in the inset of Fig. 3 is the as-implanted ^{18}O depth profile for sample no. 2 for comparison. About 3.1×10^{16} $^{18}O/cm^2$ from the gas ambient has exchanged with solid ^{16}O within the as-received YBCO film. The exchanged number is higher than that for the implanted film annealed at the same temperature (see line 7 in Fig. 1, for sample no. 9). This suggests that the surface exchange kinetics is dependent on the damage level at the surface of the film.

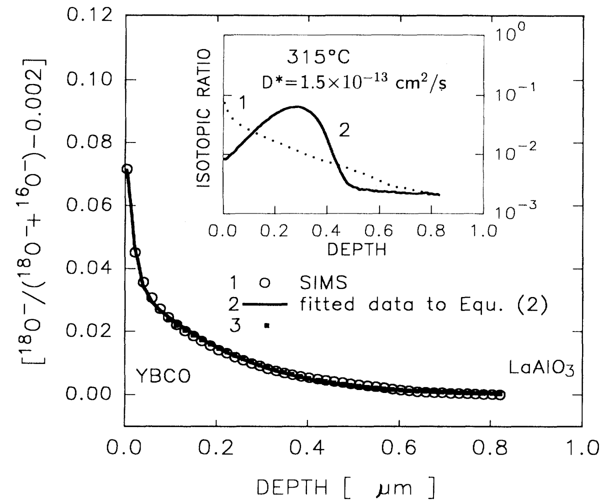

FIG. 3. Line 1, ^{18}O penetration profile along the c direction of the as-received YBCO film (sample no. 10); line 2; the fitted curve to Eq. (2); line 3, if the experimental points within the 80-nm top surface layer are ignored, the fitted curved to the first two terms in Eq. (2). Line 1 in the inset shows the ^{18}O penetration profile in another format, with the as-implanted ^{18}O isotopic ratio profile (line 2) as reference.

The isotopic profile (line 1 in Fig. 3) confirms the high mobility of oxygen within the YBCO film. This profile also shows a turning point at a depth of ~ 80 nm implying two different diffusion mechanisms. Line 2 in Fig. 3, which is very close to the experimental points, is the curve fitted to the solution appropriate for a semi-infinite solid with both volume and fast planar diffusion. The isotopic fraction C_{18} is defined as

$$C_{18}=[^{18}O^-/(^{18}O^-+^{16}O^-)-0.002]\ , \tag{1}$$

$$C_{18}=C_1\mathrm{erfc}(x/2\sqrt{D\tau})-\exp(Kx/D+K^2\tau/D)\times\mathrm{erfc}[x/(2\sqrt{D\tau})+(K/D)\sqrt{D\tau}]+C_2\exp(-C_3x^{1.2})\ , \tag{2}$$

where D is the volume diffusion coefficient. τ is the annealing time. C_1 and C_2 are constants, and C_3 is defined by

$$D_S\delta\approx 0.66C_3^{-5/3}\sqrt{4D/\tau}\ . \tag{3}$$

Here D_S is the short-circuiting (planar) diffusion coefficient (see below) and δ is the width of the short-circuiting path.[21–23] The short-circuiting paths may be thought to be grain boundaries or twin boundaries, only if the Le Claire β factor,[21] defined as $\beta\approx D_S\delta/2D\sqrt{D\tau}$, is larger than 10. From the fit to the experimental data using Eq. (2), the volume diffusion coefficient D and the surface exchange coefficient K of oxygen were found to be 1.1×10^{-15} cm^2/s and 2.3×10^{-11} cm/s, respectively. This value of diffusivity is about 4 orders of magnitude smaller than diffusion in the a-b plane but somewhat larger than expected for pure c-axis diffusion. The β factor obtained was found to be 96. It should be noted that the volume diffusion coefficient D is only applicable to the profile within the 80-nm top surface layer of the film. The short-circuit diffusion coefficient is only obtained as the product $D_S\delta$. If we let $\delta=1$ nm, the fitted D_S is found to be 4.2×10^{-12} cm^2/s.

A second method of fitting the data was also tried. If the experimental points within the 80-nm top layer are ignored, a very good fit (see line 3 in Fig. 3) can be ob-

tained to the remainder of the profile using the first two terms in Eq. (2), giving an apparent diffusivity in the deeper region D_A of 1.5×10^{-13} cm^2/s. The K_A value of 2.9×10^{-11} cm/s is only changed by a small amount. This apparent D_A value is about 1 order of magnitude smaller than that in the *a*-*b* plane of the bulk YBCO. Thus it is possible to obtain a second "good" fit using two apparent volume diffusion components, i.e., the slow one fitted to the first 80 nm and the second (fast one) to the remainder of the profile. These facts suggest that some fast diffusion paths do exist, although their nature cannot be determined from diffusion data alone. It is well known that epitaxial YBCO films usually contain defects, twin boundaries, second phase precipitates (and so some internal surfaces between them and the 123 phase), and slightly misoriented regions.[24] Any of these defects could be the source of fast diffusion paths.

IV. SUMMARY

In summary, this study shows that oxygen has a high mobility in a *c*-axis-oriented YBCO film. The apparent diffusivity of oxygen, in the *c* direction of the *c*-axis-oriented film, is much larger than that the single-crystal value in the *c* direction but smaller than that in the *a*-*b* plane. Short-circuit diffusion in the *c*-axis-oriented $YBa_2Cu_3O_{7-\delta}$ film is thought to play an important role in determining the high mobility of oxygen. This current research is being continued, and details of the relationship between the oxygen migration, the microstructure, and its evolution, and the transport properties of the irradiated YBCO film will be reported in a separate paper.

ACKNOWLEDGMENT

This work was funded by the Engineering and Physical Sciences Research Council, United Kingdom.

[1] S. J. Rothman, J. L. Routhbort, and J. E. Baker, Phys. Rev. B **40**, 8852 (1989).

[2] X. Turrillas, J. A. Kilner, I. Kontoulis, and B. C. H. Steele, J. Less-Common Met. **151**, 229 (1989).

[3] S. J. Rothman, J. L. Routbort, U. Welp, and J. E. Baker, Phys. Rev. B **44**, 2326 (1991).

[4] S. I. Bredikhin, G. A. Emel'chenko, V. Sc. Shechtman, A. A. Zhokhov, S. Carter, R. J. Chater, J. A. Kilner, and B. C. H. Steele, Physica C **179**, 286 (1991).

[5] J. Sabras, C. Dolin, J. Ayache, C. Monty, R. Maury, and A. Fert, J. Phys. (Paris) Colloq. **51**, C1-1035 (1990).

[6] Y. Ikuma and S. Akiyoshi, J. Appl. Phys. **64**, 3915 (1988).

[7] Y. X. Chen, J. Zhang, and Z. Wu, Supercond. Sci. Technol. **5**, 463 (1992).

[8] S. H. Lee, S. C. Bae, K. K. Ku, and H. J. Shin, Phys. Rev. B **46**, 9142 (1992).

[9] Hans-Ulrich Krebs, C. Krauns, and F. Matteis, J. Alloys Comp. **195**, 203 (1993).

[10] X. X. Xi, G. Linker, O. Meyer, E. Nold, B. Obst, F. Ratzel, R. Smithey, B. Strehlau, F. Weschenfelder, and J. Geerk, Z. Phys. B **74**, 13 (1989).

[11] F. J. Muller, J. C. Gallop, and A. D. Caplin, Supercond. Sci. Technol. **4**, 616 (1991).

[12] Yupu Li, J. A. Kilner, T. J. Tate, M. J. Lee, F. M. Saba, L. F. Cohen, A. D. Caplin, and P. G. Quincey, J. Appl. Phys. **75**, 4081 (1994).

[13] Yupu Li, J. A. Kilner, T. J. Tate, M. J. Lee, F. M. Saba, L. F. Cohen, A. D. Caplin, and P. G. Quincey, Nucl. Instrum. Methods B **85**, 281 (1994).

[14] J. F. Ziegler, J. P. Biersack, and U. Littmark, *The Stopping and Ranges of Ion in Solids* (Pergamon, New York, 1985).

[15] T. J. Tate, M. J. Lee, Yupu Li, J. A. Kilner, Y. H. Li, C. Leach, D. Leach, A. D. Caplin, R. E. Somehk, P. Przyslupski, and P. G. Quincey, Physica C **235-240**, 569 (1994).

[16] L. E. Rehn, Nucl. Instrum. Methods B **64**, 161 (1992).

[17] O. Meyer, T. Kroener, J. Remmel, J. Geerk, G. Linker, B. Strehlau, and Th. Wolf, Nucl. Instrum. Methods B **65**, 539 (1992).

[18] G. J. Clark, A. D. Marwick, R. H. Koch, and R. B. Laibowitz, Appl. Phys. Lett. **51**, 139 (1987).

[19] J. D. Jorgensen, M. A. Beno, D. G. Hinks, L. Soderholm, K. J. Volin, R. L. Hitterman, J. D. Grace, I. K. Schuller, C. U. Segre, K. Zhang, and M. S. Kleefisch, Phys. Rev. B **36**, 3608 (1987).

[20] See, for example, W. Jost, *Diffusion in Solids, Liquid, and Gases* (Academic, New York, 1960).

[21] A. D. Le Claire, Brit. J. Appl. Phys. **14**, 351 (1963).

[22] Y. Fang and J. L. Routbort, J. Appl. Phys. **75**, 210 (1994).

[23] J Crank, *The Mathematics of Diffusion* (Oxford University Press, London, 1956).

[24] H. J. Scheel, M. Berkowqski, and B. Chabot, J. Crystal Growth **115**, 19 (1990).